UNIVERSITY of York

This is a repository copy of *Critical Delocalization of Chiral Zero Energy Modes in Graphene*.

White Rose Research Online URL for this paper:
https://eprints.whiterose.ac.uk/124218/

Version: Published Version

Article:
Ferreira, Aires orcid.org/0000-0001-6017-8669 and Mucciolo, Eduardo (2015) Critical Delocalization of Chiral Zero Energy Modes in Graphene. Physical Review Letters. 106601. ISSN 1079-7114

https://doi.org/10.1103/PhysRevLett.115.106601

Reuse
Items deposited in White Rose Research Online are protected by copyright, with all rights reserved unless indicated otherwise. They may be downloaded and/or printed for private study, or other acts as permitted by national copyright laws. The publisher or other rights holders may allow further reproduction and re-use of the full text version. This is indicated by the licence information on the White Rose Research Online record for the item.

Takedown
If you consider content in White Rose Research Online to be in breach of UK law, please notify us by emailing eprints@whiterose.ac.uk including the URL of the record and the reason for the withdrawal request.

White Rose university consortium
Universities of Leeds, Sheffield & York

eprints@whiterose.ac.uk
https://eprints.whiterose.ac.uk/

Critical Delocalization of Chiral Zero Energy Modes in Graphene

Aires Ferreira*
Department of Physics, University of York, York YO10 5DD, United Kingdom

Eduardo R. Mucciolo
Department of Physics, University of Central Florida, Orlando, Florida 32816, USA

(Received 9 July 2015; published 31 August 2015)

Graphene subjected to *chiral*-symmetric disorder is believed to host zero energy modes (ZEMs) resilient to localization, as suggested by the renormalization group analysis of the underlying nonlinear sigma model. We report accurate quantum transport calculations in honeycomb lattices with in excess of 10^9 sites and fine meV resolutions. The Kubo dc conductivity of ZEMs induced by vacancy defects (chiral BDI class) is found to match $4e^2/\pi h$ within 1% accuracy, over a parametrically wide window of energy level broadenings and vacancy concentrations. Our results disclose an unprecedentedly robust metallic regime in graphene, providing strong evidence that the early field-theoretical picture for the BDI class is valid well beyond its controlled weak-coupling regime.

DOI: 10.1103/PhysRevLett.115.106601 PACS numbers: 72.80.Vp, 73.22.Pr, 73.23.-b, 73.63.-b

After more than half a century, Anderson localization remains a central concept in condensed matter physics, with its many ramifications providing new insights into the behavior of disordered electrons [1]. The discovery of the "tenfold" symmetry classes of disordered metals [2,3]—beyond the standard threefold Wigner-Dyson classification scheme—has revealed a surprisingly rich diagram of Anderson localization transitions, including multifractality and critical delocalization in low dimensions [4].

The interest in critical quantum transport in two-dimensional (2D) systems has been greatly amplified with the discovery of graphene, a one-atom-thick crystal endowed with massless Dirac fermions [5]. The internal pseudospin of the Dirac fermions—stemming from the honeycomb lattice structure with two sublattices—enables a rich variety of quantum transport phenomena [6,7], including minimum conductivity in the clean limit [8], and crossover from weak-localization—orthogonal class—to weak-antilocalization—symplectic class—with increasing impurity potential range [9].

Recently, disordered graphene in the *chiral* symmetry class has been the focus of much attention [10–13]. In chiral models defined on bipartite lattices, disordered wave functions come in electron-hole pairs with energies $\pm E$ linked by a unitary matrix diagonal in the sublattice space, i.e., $|\phi_\pm\rangle = \hat{\sigma}_z|\phi_\mp\rangle$. A remarkable feature of the chiral class is the existence of *critical* states at the band center—zero-energy modes (ZEMs)—possessing multifractal statistics and an absence of weak localization corrections at all orders in perturbation theory [2]. In graphene, the simplest realization of critical ZEMs is provided by randomly distributed vacancies. A vacancy is a topological defect obtained by cutting out all adjacent bonds to a given carbon site. Vacancies drastically affect the spectrum near the Dirac point, leading to the appearance of ZEMs with enhanced density of states (DOS) and quasilocalized character [14,15], which can be detected by scanning tunneling microscopy [16]. Other examples of chiral-symmetric disorder in graphene include random non-Abelian gauge fields (ripples) [17], and resonant scatterers (e.g., adsorbed hydrogen) [18]. Whether quantum criticality induced by chiral disorder could explain the resilience of the minimum conductivity of graphene to Anderson localization is an outstanding question.

The focus of this Letter is on vacancy-induced ZEMs, recently implicated in a controversy regarding the exact nature of the quantum transport at the Dirac point [19–22]. Vacancy-defective graphene belongs to the chiral orthogonal ensemble (class BDI in the Altland-Zirnbauer classification of random fermion models [3]). The vanishing of the β function of the effective nonlinear sigma model (NLσM) led Ostrovsky *et al.* to conjecture a line of fixed points with nonuniversal metallic conductivity of the order of the conductance quantum $\sigma(0) \approx e^2/h$ [22–24]. However, the validity of the NLσM of the BDI class has been questioned, as vacancies are infinitely strong scatterers, not amenable to perturbative analysis [12]. On the other hand, numerical evaluations of the conductivity using wave-packet propagation methods show localization of all states $\sigma(E) \to 0$, including the ZEMs [19–21]. The Gade singularity in the DOS approaching $E \to 0$ [12], however, raises questions on the validity of the extraction of the conductivity using wave-packet propagation methods.

In this Letter we report on accurate calculations of the longitudinal dc conductivity in macroscopic large disordered graphene. By employing an *exact* representation of the Kubo formula in terms of Chebyshev polynomials, we were able to extract the behavior of $\sigma(E)$ at the Dirac point

 © 2015 American Physical Society

with unprecedented resolution. Our results univocally show that vacancy-induced ZEMs display critical delocalization, as suggested by perturbative calculations based on the NLσM [22–24] and numerical studies of the two-terminal conductance in nanoribbons with resonant scalar impurities [22,23]. We find a *constant* conductivity over a wide range of vacancy concentrations,

$$\sigma(0) = \sigma_{\mathrm{ZEM}}(1.00 \pm 0.01), \qquad \sigma_{\mathrm{ZEM}} \equiv \frac{4e^2}{\pi h}.$$

Strikingly, the ZEM conductivity is found to be robust with respect to variations in the inelastic broadening parameter η entering in the disordered Green functions down to $\eta = 2.5$ meV. This result is very surprising as vacancies are the ultimate case of a strong short-range disorder in graphene mixing K and K' valleys [6,7].

The model.—Chiral disordered graphene is modeled by the standard tight-binding Hamiltonian of π electrons defined on a honeycomb lattice

$$\hat{H} = -t \sum_{\langle i,j \rangle} (\hat{a}_i^\dagger \hat{b}_j + \hat{b}_j^\dagger \hat{a}_i), \tag{1}$$

where $\langle i, j \rangle$ denotes nearest-neighbor pairs of carbon atoms and $t = 2.7$ eV is the corresponding hopping integral [5]. Periodic boundary conditions along zigzag and armchair directions are employed. The vacancies—obtained by removing the corresponding p_z orbitals—are distributed randomly on both sublattices with overall concentration n_i. In what follows, we briefly outline the Chebyshev-polynomial Green function (CPGF) method used to accurately evaluate spectral properties and response functions of real size systems.

The CPGF approach.—The numerical evaluation of the lattice resolvent operator $\hat{\mathcal{G}}(z) = (z - \hat{H})^{-1}$ requires a nonzero broadening (*resolution*) parameter $\eta = \mathrm{Im}\, z \gtrsim \delta E$, where δE is the mean level spacing. We are interested in the limit of small δE, where strong quantum interference effects associated with ZEMs can be fully appreciated [4]. Numerical evaluations of disordered lattice Green functions in the presence of critical states are computationally highly demanding. In Ref. [12] a time-domain stochastic method has been employed to extract the DOS with high resolution. Here, we evaluate target functions directly in the energy domain by expressing Green functions in terms of an *exact* polynomial expansion. Our approach turns out to be particularly advantageous in the calculation of the conductivity (see below). First-kind Chebyshev polynomials $\{T_n(x)\}_{n \in \mathbb{N}_0}$ are employed due to their superior convergence properties [25,26]. The use of Chebyshev polynomials as a basis set requires rescaling the spectrum of $\hat{H}$ into the interval $[-1:1]$. To this end, we scale both operators and energy variables, $\hat{H} \to \hat{h} = \hat{H}/W$, $\epsilon = E/W$, and $\lambda = \eta/W$, where W is the half-bandwidth. With this notation the Green function admits the following representation:

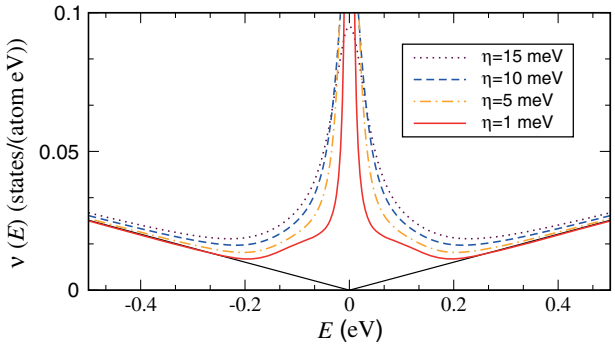

FIG. 1 (color online). Density of states of disordered graphene as a function of Fermi energy. The Gade singularity of ZEMs is apparent as the energy levels are probed with increasing resolution $\eta \to 0$. The pristine DOS is shown (black line) as a guide to the eye.

$$\hat{\mathcal{G}}(E + i\eta) = \frac{1}{W} \sum_{n=0}^{\infty} g_n(\epsilon, \lambda) \mathcal{T}_n(\hat{h}), \tag{2}$$

where $\{\mathcal{T}_n(\hat{h})\}$ are defined through the Chebyshev recursion relations: $\mathcal{T}_0(\hat{h}) = \hat{\mathbb{1}}$, $\mathcal{T}_1(\hat{h}) = \hat{h}$, and $\mathcal{T}_{n+1}(\hat{h}) = 2\hat{h} \cdot \mathcal{T}_n(\hat{h}) - \mathcal{T}_{n-1}(\hat{h})$. The coefficients $\{g_n(\epsilon, \lambda)\}_{n \in \mathbb{N}_0}$ are system independent and possess a simple closed form [27]. The CPGF expansion [Eq. (2)] is the starting point of the accurate calculations reported in this work.

Density of states.—We start with a brief discussion of the DOS. Formally,

$$\nu(E) = -\frac{g_s}{\pi D} \mathrm{Tr}\, \overline{\mathrm{Im}\, \hat{\mathcal{G}}(E + i\eta)}, \tag{3}$$

where $g_s = 2$ accounts for spin degeneracy and the bar means disorder averaging. According to Eqs. (2) and (3), the information about the DOS is contained in the Chebyshev moments $\nu_n = \mathrm{Tr}\, \mathcal{T}_n(\hat{h})$ of individual disorder realizations. To probe features induced by chiral ZEMs with meV resolution, we consider a honeycomb lattice with $D = 60000 \times 60000$ sites ($\approx 94\ \mu\mathrm{m}^2$). This system has $\delta E \approx 0.3$ meV at the Dirac point in the absence of vacancies. The DOS for a dilute vacancy concentration $n_i = 0.4\%$ is shown in Fig. 1. Given the large size of the system simulated, one disorder configuration is sufficient to obtain very precise results. The expected enhancement of the DOS associated with ZEMs near $E = 0$ [14,15] is seen to dramatically depend on the resolution. Extracting the exact scaling as $E \to 0$ is a demanding task as the number of Chebyshev moments required to converge the DOS, i.e., $N \propto W/\eta$, can be of the order of several tens of thousands even for meV resolution; here, $N = 15 \times 10^3$. (Similar technical challenges were encountered in Ref. [12].) The analysis of the data suggests that the singularity is stronger than that predicted by Gade and Wegner [2] in full consistency with the detailed numerical study of

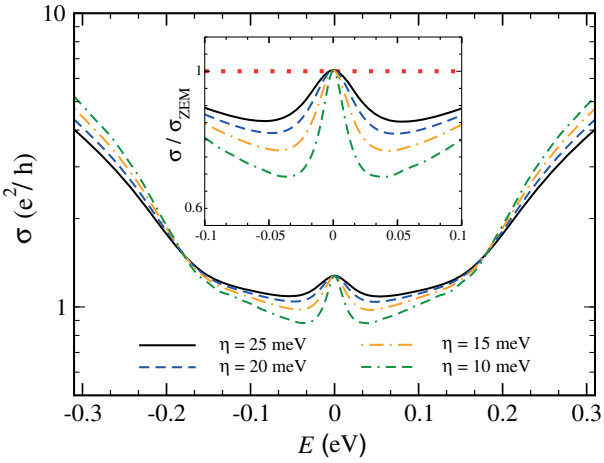

FIG. 2 (color online). Fully converged Kubo dc conductivity for a 0.4% vacancy concentration as a function of Fermi energy at selected values of η. The calculation required $N^2 = 6.4 \times 10^7$ Chebyshev moments. The inset shows a zoom of the peak at the Dirac point. Statistical fluctuations of the data are within $\simeq 1\%$.

Ref. [12] and the analytical results in Ref. [13]; see Supplemental Material for full details [27].

Conductivity.—The finite-size Kubo formula reads

$$\sigma(E) = \frac{2\hbar e^2}{\pi\Omega} \mathrm{Tr}\left[\overline{\mathrm{Im}\,\hat{\mathcal{G}}\,(E+i\eta)\,\hat{v}_\parallel\,\mathrm{Im}\,\hat{\mathcal{G}}\,(E+i\eta)\,\hat{v}_\parallel}\right], \tag{4}$$

where $\hat{v}_\parallel = [\hat{r}_\parallel, \hat{H}]/i\hbar$ is the velocity operator (taken along the zigzag direction) and Ω is the area. Here, the broadening η mimics the effect of uncorrelated inelastic scattering processes, thus defining a time scale $\tau_i = \hbar/\eta$ for phase coherence in the system [32,33].

The calculation of $\sigma(E)$ follows identical steps as outlined for the DOS. The presence of two Green functions in Eq. (4) requires a double polynomial expansion, rendering the calculation computationally extremely demanding. Analogously to the kernel polynomial method [18,25], the full spectral information is now contained in the Chebyshev moments $\sigma_{nm} = \mathrm{Tr}\,[\mathcal{T}_n\,(\hat{h})\,\hat{v}_\parallel\,\mathcal{T}_m\,(\hat{h})\,\hat{v}_\parallel]$. The number of moments required ($\equiv N^2$) depends on the desired resolution. Typically, $N \approx 10 \times (W/\eta)$ converges the conductivity to two decimal places. From the knowledge of $\{\sigma_{nm}\}$ the dc conductivity $\sigma(E)$ is quickly reconstructed. See Ref. [27] for details.

Full spectral results.—We first provide a bird's-eye view of $\sigma(E)$ before specializing to the case of ZEMs. For modest resolutions, $\eta \gtrsim 10$ meV, the physically meaningful limit $\sigma_{\Omega\to\infty}(E)$ is achievable in relatively small systems with $D \approx 10^7$. The fully converged dc conductivity for a dilute vacancy concentration $n_i = 0.4\%$ is shown in Fig. 2. The behavior of $\sigma_{\Omega\to\infty}(E)$ with decreasing η (i.e., increasing τ_i) provides direct information on the quantum transport regime [e.g., $\lim_{\eta\to 0}\sigma_{\Omega\to\infty}(E) = 0(>0)$ in the insulating (metallic) phase] [33]. The limit $\Omega \to \infty$ is implicit hereafter. In an energy window $\simeq \pm 0.2$ eV around $E = 0$—excluding the Dirac point itself—$\sigma(E)$ *decreases* as η is lowered, showing that localization effects become increasingly more important as the thermodynamic limit $\eta \to \delta E \to 0$ is approached. The effect is notably stronger in the vicinity of the Dirac point, where strong localization ($\sigma \lesssim e^2/h$) takes place already for $\eta \approx 10$ meV. This indicates that the *a priori unknown* simulated inelastic lengths $L_i = L_i(E, \tau_i)$ are sufficiently large that charge carriers can effectively experience localization. In contrast, at energies $|E| \gtrsim 0.2$ eV an *increase* of $\sigma(E)$ with increasing τ_i is observed. This suggests that at such energies the simulated L_i is not yet sufficiently large to observe localization effects. This interpretation is further confirmed below. At the Dirac point, on the other hand, $\sigma(E)$ seems insensitive to the inelastic broadening parameter, matching σ_{ZEM} with 1% precision in the entire range (see inset to Fig. 2). The anomalous robustness of the dc conductivity as $E \to 0$ is highly suggestive of a quantum critical point, in agreement with field-theoretical predictions [24].

High resolution results.—To probe the extension of delocalization effects at the Dirac point, we devise a scheme to enable the computation of $\sigma(E)$ with meV resolution. First, we recursively construct the vectors

$$|\varphi_\pm(E)\rangle = \frac{1}{W}\sum_{n=0}^{\infty} \mathrm{Im}\,[g_n(\epsilon,\lambda)]\hat{\mathcal{O}}_\pm^n|\varphi\rangle, \tag{5}$$

where $|\varphi\rangle = \sum_{i=1}^{D}\chi_i|i\rangle$ is a real random vector, $\hat{\mathcal{O}}_+^n = \mathcal{T}_n(\hat{h})\hat{v}_\parallel$, and $\hat{\mathcal{O}}_-^n = \hat{v}_\parallel\mathcal{T}_n(\hat{h})$. The random variables $\{\chi_i\}$ are uncorrelated and taken from a uniform distribution with $\langle\!\langle \chi_i \rangle\!\rangle = 0$. The series is truncated at $n < N$ when convergence to the desired precision is achieved. Finally, the Kubo dc conductivity is obtained from

$$\sigma_\varphi(E) = \frac{2\hbar e^2}{\pi\Omega}\langle\varphi_-(E)|\varphi_+(E)\rangle, \tag{6}$$

by averaging with respect to both disorder and random vector realizations, i.e., $\sigma(E) = \langle\!\langle\overline{\sigma_\varphi(E)}\rangle\!\rangle$ [27]. We note that for ZEMs, Eq. (5) acquires a particular simple form, $|\varphi_\pm(0)\rangle = W^{-1}\sum_n \mathrm{Im}[g_{2n}(0,\lambda)]\hat{\mathcal{O}}_\pm^{2n}|\varphi\rangle$. The advantage of Eqs. (5) and (6) is that they do not require calculation of individual Chebyshev moments $\{\sigma_{nm}\}$ (cost $\propto N^2$). In practice, this allows us to reach fine resolution (higher N) and also much larger systems containing up to a few billion lattice sites [34].

The high-resolution conductivity data across the various transport regimes identified earlier are given in Fig. 3. For convenience, we define an *effective* system size $L_* \equiv \hbar\pi v_F/\eta$ as the length of a pristine graphene system having $\delta\epsilon = \eta$ at the Dirac point. The largest simulation has

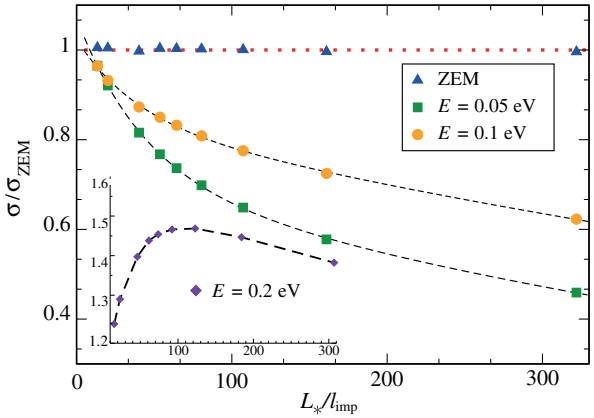

FIG. 3 (color online). Fully converged Kubo dc conductivity for a 0.4% vacancy concentration as a function of L_*/l_{imp} at selected energies. Here $l_{\mathrm{imp}} \simeq 2.24$ nm is the average distance between vacancies. A large honeycomb lattice with 3.6×10^9 sites was simulated to obtain good precision at large L_*. Statistical fluctuations of the data are within $\simeq 1\%$.

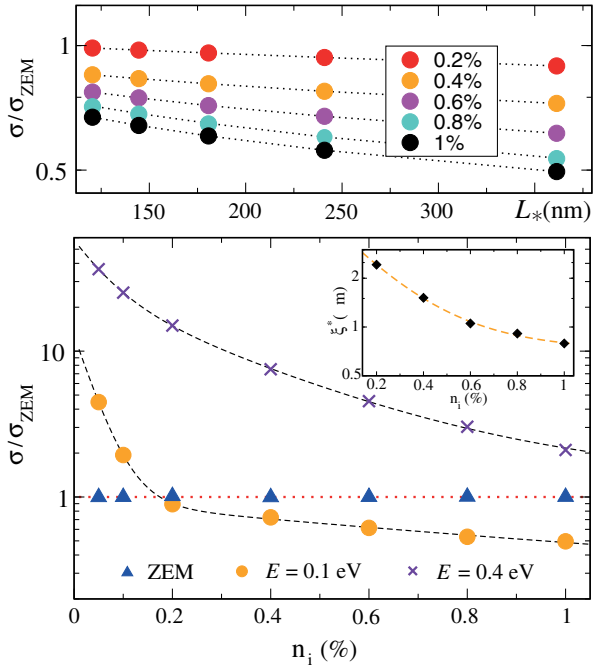

FIG. 4 (color online). Impact of vacancy concentration on bulk transport. Top panel: localization of states with $E = 0.1$ eV as a function of L_* at various vacancy concentrations. Bottom panel: variation of $\sigma(E)$ with n_i at selected energies.

$L_* \simeq 0.7$ μm, corresponding to a broadening of only 2.5 meV. The state vectors in Eq. (5) were calculated with $N = 12000$ Chebyshev iterations. The ZEM conductivity shows no sign of localization, being numerically very close to $\sigma_{\mathrm{ZEM}} = 4e^2/(\pi h)$ through a parametrically wide range of inelastic broadenings in the range [2.5,60] meV. This is to be contrasted with the behavior of $\sigma(E)$ away from the band center. For instance, at energies $E = \{50, 100\}$ meV there is a strong suppression towards $\sigma \to 0$ as L_* increases. The localization is stronger in the neighborhood of the critical point at zero energy, with states with $E = 50$ meV localizing first than those having $E = 100$ meV. This behavior can also be inferred from Fig. 2, which shows that the tendency as $\eta \to 0$ ($L_* \to \infty$) is for states to localize first in the vicinity of the ZEMs. In the inset to Fig. 3 the behavior for an energy far away from the Dirac point is shown. A transition from ballistic to localized regime is observed as L_* increases. Eventually, as $L_* \to \infty$, all states with $E \neq 0$ become localized. The latter is consistent with the behavior expected for random fermions in the BDI class [1,4]. Crucially, however, our accurate numerical treatment shows that the chiral symmetry at $E = 0$ protects ZEMs from localization up to $L_* \approx 1$ μm. This exotic 2D metallic regime had been predicted by the renormalization group (RG) analysis of the NLσM for the BDI class [24], although a fully nonperturbative calculation of the microscopic conductivity able to capture strong quantum interference effects at the Dirac point was lacking until now.

Universal ZEM conductivity.—We finally investigate the robustness of the ZEMs metallic conductivity against changes in vacancy concentration. According to the perturbative RG analysis for white-noise disorder in the BDI class, $\sigma(0)$ should depend weakly on the disorder strength [24]. The actual picture for vacancies—being infinitely strong scatterers—is difficult to predict based solely on field-theoretical methods [12,35]. The little sensitivity of $\sigma(0)$ to the effective length L_* intuitively suggests a small dependence with the defect concentration too. Interestingly, numerical results for transport across narrow graphene strips show $\sigma(0) \approx \sigma_{\mathrm{ZEM}}$ with weak dependence on n_i [23], demonstrating that, although evanescent modes are strongly affected by scattering from vacancy defects, the large number of modes available (large DOS) counteracts perfectly to restore graphene's clean ballistic conductivity [8]. To investigate the possibility of a disorder-induced universal metallic regime in graphene, we perform accurate Kubo calculations over 2 orders of magnitude in n_i. We take a fine broadening $\eta = 2.5$ meV so as to guarantee that L_* is sufficiently large to capture any marked localization trend near the Dirac point. Our results are summarized in Fig. 4. Away from the band center the conductivity is strongly decaying with n_i as expected. For instance, at $E = 0.1$ eV—a typical Fermi energy in experiments—the conductivity swiftly enters in the strong localized regime already for dilute concentrations $n_i \approx 0.2\%$. The dependence of $\sigma(E)$ with L_* is well fitted by an exponential law $\sigma \propto e^{-L_*/\xi_*}$; see top panel. (The dependence of ξ_* with the defect concentration is shown in the inset to the bottom panel.) However, at the band center ZEMs show no signs of localization even beyond the very dilute limit up to concentrations $n = 1\%$. For completeness we provide

the results for $E = 0.4$ eV where transport is ballistic in the simulated range of L_* up to $n \approx 0.8\%$ (see also Fig. 3).

We briefly comment on previous wave-packet propagation calculations reporting on $\sigma(0) \to 0$ [19–21]. The strong singularity of the DOS at $E = 0$ makes the numerical extraction of the conductivity from the Einstein relation for diffusive transport $\sigma(E) \propto \nu(E)D(E)$ very challenging. Additionally, the level broadening inserted as the inverse of the time cutoff in the wave packet propagation may not be equivalent to the broadening employed in the finite-size Kubo formula [Eq. (4)]. Although computationally much more demanding, our approach has the advantage of assessing directly the microscopic conductivity with no further assumptions.

In summary, we have demonstrated critical delocalization of zero energy modes in graphene by means of accurate numerical evaluations of the Kubo conductivity in real size disordered systems containing billions of carbon atoms. Rather remarkably, the absence of localization in the BDI class at the Dirac point is consistent with nonlinear sigma model predictions [24] and numerical studies of the Dirac equation [22,23], suggesting an unprecedentedly robust metallic state in two dimensions. We hope that our work encourages further use of accurate large-scale polynomial methods in the study of Anderson localization transitions.

A. F. acknowledges M.D. Costa for technical discussions and high-performance computing (HPC) support. The calculations were performed in HPC facilities based at the Graphene Research Centre, National University of Singapore. A. F. is thankful for the partial support from the National Research Foundation, Prime Minister Office, Singapore, under its Competitive Research Programme (Grant No. R-144-000-295-281). A. F. gratefully acknowledges the financial support of the Royal Society (U.K.) through a Royal Society University Research Fellowship.

*Corresponding author.
aires.ferreira@york.ac.uk

[1] *50 Years of Anderson Localization*, edited by E. Abrahams (World Scientific, Singapore, 2010).
[2] R. Gade and F. Wegner, Nucl. Phys. **B360**, 213 (1991); R. Gade, Nucl. Phys. **B398**, 499 (1993).
[3] M. R. Zirnbauer, J. Math. Phys. (N.Y.) **37**, 4986 (1996); A. Altland and M. R. Zirnbauer, Phys. Rev. B **55**, 1142 (1997).
[4] F. Evers and A. D. Mirlin, Rev. Mod. Phys. **80**, 1355 (2008).
[5] A. H. Castro Neto, F. Guinea, N. M. R. Peres, K. S. Novoselov, and A. K. Geim, Rev. Mod. Phys. **81**, 109 (2009).
[6] N. M. R. Peres, Rev. Mod. Phys. **82**, 2673 (2010).
[7] E. R. Mucciolo and C. H. Lewenkopf, J. Phys. Condens. Matter **22**, 273201 (2010).
[8] M. I. Katsnelson, Eur. Phys. J. B **51**, 157 (2006).
[9] H. Suzuura and T. Ando, Phys. Rev. Lett. **89**, 266603 (2002).
[10] L. Schweitzer and P. Markoš, Phys. Rev. B **85**, 195424 (2012).
[11] G. Usaj, P. S. Cornaglia, and C. A. Balseiro, Phys. Rev. B **89**, 085405 (2014).
[12] V. Hafner, J. Schindler, N. Weik, T. Mayer, S. Balakrishnan, R. Narayanan, S. Bera, and F. Evers, Phys. Rev. Lett. **113**, 186802 (2014).
[13] P. M. Ostrovsky, I. V. Protopopov, E. J. Konig, I. V. Gornyi, A. D. Mirlin, and M. A. Skvortsov, Phys. Rev. Lett. **113**, 186803 (2014).
[14] V. M. Pereira, F. Guinea, J. M. B. Lopes dos Santos, N. M. R. Peres, and A. H. Castro Neto, Phys. Rev. Lett. **96**, 036801 (2006).
[15] V. M. Pereira, J. M. B. Lopes dos Santos, and A. H. Castro Neto, Phys. Rev. B **77**, 115109 (2008).
[16] M. M. Ugeda, I. Brihuega, F. Guinea, and J. M. Gomez-Rodriguez, Phys. Rev. Lett. **104**, 096804 (2010).
[17] D. Huertas-Hernando, F. Guinea, and A. Brataas, Phys. Rev. Lett. **103**, 146801 (2009).
[18] A. Ferreira, J. Viana-Gomes, J. Nilsson, E. R. Mucciolo, N. M. R. Peres, and A. H. Castro Neto, Phys. Rev. B **83**, 165402 (2011).
[19] Z. Fan, A. Uppstu, and A. Harju, Phys. Rev. B **89**, 245422 (2014).
[20] G. Trambly de Laissardiere and D. Mayou, Phys. Rev. Lett. **111**, 146601 (2013).
[21] A. Cresti, F. Ortmann, T. Louvet, D. Van Tuan, and S. Roche, Phys. Rev. Lett. **110**, 196601 (2013).
[22] S. Gattenlohner, W.-R. Hannes, P. M. Ostrovsky, I. V. Gornyi, A. D. Mirlin, and M. Titov, Phys. Rev. Lett. **112**, 026802 (2014).
[23] P. M. Ostrovsky, M. Titov, S. Bera, I. V. Gornyi, and A. D. Mirlin, Phys. Rev. Lett. **105**, 266803 (2010).
[24] P. M. Ostrovsky, I. V. Gornyi, and A. D. Mirlin, Phys. Rev. B **74**, 235443 (2006).
[25] A. Weisse, G. Wellein, A. Alvermann, and H. Fehske, Rev. Mod. Phys. **78**, 275 (2006).
[26] J. P. Boyd, 2nd ed. *Chebyshev and Fourier Spectral Methods* (Dover Publications, New York, 2001).
[27] See Supplemental Material at http://link.aps.org/supplemental/10.1103/PhysRevLett.115.106601 for details on the Chebyshev-polynomial Green function (CPGF) method as well as a thorough description of the accurate large-scale numerical calculations presented in the Letter, which includes Refs. [28–31].
[28] A. Ferreira (to be published).
[29] H. Tal-Ezer and R. Kosloff, J. Chem. Phys. **81**, 3967 (1984).
[30] I. S. Gradshteyn and I. M. Ryzhik, 7th ed. *Table of Integrals, Series, and Products* (Elsevier, Academic Press, New York, 2007).
[31] T. Iitaka and T. Ebisuzaki, Phys. Rev. E **69**, 057701 (2004).
[32] D. J. Thouless and S. Kirkpatrick, J. Phys. C **14**, 235 (1981).
[33] Y. Imry, *Introduction to mesoscopic physics*, 2nd edition (Oxford University Press, New York, 2002).
[34] A single realization of a system with $D = 3.6 \times 10^9$ atoms with N up to 12 000 takes only a few days of HPC time if enough memory (typically 0.5 TB) is available to recursively construct the huge vectors $|\varphi_{\pm}(E)\rangle$ on the fly.
[35] E. J. Konig, P. M. Ostrovsky, I. V. Protopopov, and A. D. Mirlin, Phys. Rev. B **85**, 195130 (2012).